Clays and Clay Minerals, Vol. 52, No. 5, 622–634, 2004.

VERY LOW-TEMPERATURE ALTERATION OF SIDEROMELANE IN HYALOCLASTITES AND HYALOTUFFS FROM KILAUEA AND MAUNA KEA VOLCANOES: IMPLICATIONS FOR THE MECHANISM OF PALAGONITE FORMATION

AHMED DRIEF* AND PETER SCHIFFMAN

Department of Geology, University of California, Davis, California 95616, USA

Abstract—Three petrographically distinct styles of altered glasses in two hyaloclastites and one hyalotuff were studied. The texture and chemistry of these samples were investigated using electron probe microanalysis, scanning electron microscopy and transmission electron microscopy in order to understand better the mechanism by which alteration of sideromelane and formation of palagonite occurred in these samples. The results show that clay minerals (primarily smectites) are present in three different microenvironments: (1) coating the surfaces of glass and crystals or vesicle walls; (2) as a relatively heterogeneous, but well crystallized, replacement product (*i.e*. reddened smectite grain replacement or RSGR) of glass or; (3) as a relatively homogeneous, amorphous to poorly crystalline replacement product (*i.e*. palagonite). Both the grain size and composition of these smectite-like materials vary considerably.

Crystalline smectites occur in both hyaloclastites and have an intermediate composition between the two end-members nontronite and saponite. This composition could correspond to a mechanical intergrowth and/or an interstratification of two different smectites: one dioctahedral (*i.e*. nontronite) and one trioctahedral (*i.e*. saponite or stevensite) or simply to a true di-trioctahedral smectite. The coating smectite appears to have precipitated by a paragenetically-early, dissolution-precipitation mechanism prior to the formation of the RSGR. The high Ti content found in RSGR is attributable to an amorphous Ti-rich material which is intergrown with smectite and which behaves as a sink for immobile elements and those not included in smectite.

Palagonite from both hyaloclastites and hyalotuff is poorly to non-crystalline and more aluminous than the coating smectites. Palagonite from the hyalotuff has an Fe-rich montmorillonite-like composition. The TEM images show a 30–50 nm thick leached layer formed by selective (non-stoichiometric) dissolution that takes place in the fracture domain. The hydration and replacement of glass during the palgonitization process is accompanied by the loss of Fe, Mg and Ca with a concomitant gain of Al. Both palagonites (from hyaloclastites and hyalotuff) show smilar textural and chemical characteristics.

Key Words—Congruent, Dissolution, Incongruent, Leached Layer, Montmorillonite, Nontronite, Palagonite, Saponite, Smectite, TEM.

INTRODUCTION

Although first described by Von Waltershausen (1845), palagonite is still an inconclusively characterized material. Peacock (1926) delineated two forms of palagonite: "gel" – an amorphous variety, and "fibro" – a weakly crystalline form. The term palagonite was commonly used to describe any hydrous alteration product of mafic glass or any crystalline material that evolves from the palagonite itself (Furnes, 1984; Jakobsson, 1972; Jercinovic *et al*., 1990; Thorseth *et al*., 1991). Honnorez (1978) recognized that the term 'palagonite' had been used differently in various studies and recommended that the term 'palagonitized glass' be used to describe altered basaltic glass. More recently, Stroncik and Schminke (2001) recommended that fibropalagonite not be used and what has been called gel-palagonite simply be called palagonite. Reviews by Honnorez (1981), Fisher and Schmincke (1984), Singer and Banin (1990), and Stroncik and Schminke (2001) have summarized the considerable literature on the usage of the term palagonite, the formation of palagonite, and compositional changes attending the formation of palagonite. In the present study the term 'palagonite' refers to what was described as gel-palagonite material that replaces sideromelane (Stroncik and Schminke 2001) and reddened smectite grain replacement (RSGR) refers to what was described in the past as fibropalagonite (Walton and Schiffman 2003).

At low temperature and in an aqueous environment, sideromelane is an unstable material that alters to a hydrated, heterogeneous material that may be X-ray amorphous or consist of poorly crystalline clay minerals (Moore, 1966; Stokes, 1971). Many palagonite workers have indicated that palagonitized glass contains a smectite-like structure (*e.g*. Hay and Iijima, 1968a; Singer, 1974; Eggleton and Keller, 1982; Zhou *et al*., 1992), even in the initial stages of sideromelane alteration. Eggleton and Keller (1982) noted the

* E-mail address of corresponding author:
drief@geology.ucdavis.edu
DOI: 10.1346/CCMN.2004.0520508

compositional similarity between palagonite and smectite when electron microprobe spot analyses were recalculated to a cation charge of 22, and concluded that palagonite is composed mainly of dioctahedral smectite with significant Mg content in the octahedral sheet. Conversely, some workers, especially from the Planetary Science community, have suggested that smectite is not an essential component of 'palagonite' (*e.g.* Gooding and Keil; 1978; Bell *et al*., 2000; Morris *et al*., 2001). Different mineralogical complexes have been proposed to describe palagonite. Hay and Iijima (1968b) proposed that palagonite is composed of montmorillonite and mixed-layer mica-montmorillonite. Other authors have suggested the presence of kaolinite, illite, mixed-layer clay minerals or zeolites (Furnes, 1984). Zhou and Fyfe (1989) reported that fibropalagonite was composed of stevensitic smectite, whereas related fracture-filling authigenic minerals included smectite clays, phillipsite, calcite and Fe and Mn oxides.

Recent experimental studies on the low-temperature alteration of sideromelane have attempted to determine the mechanism responsible for palagonite formation. Different models such as selective (Berger *et al*., 1987; Thomassin *et al*., 1983) or congruent (*e.g.* Crovisier *et al*., 1987) dissolution of the glass have been proposed. The experimental results of Berger *et al*. (1987) suggested the initial formation of a leached layer which shows no apparent signs of alteration and/or recrystallization. In these experiments, further leaching of Si was thought to create a porous structure through which cations in solution diffuse and form a silica gel which subsequently crystallized to saponite. According to Crovisier *et al*. (1987), one can expect three possibilities during the palagonitization process, starting with congruent or selective dissolution of the glass:

(1) The dissolution is congruent. If there is no significant change in pH, the rate of silica release will be constant and silica concentration in the solution will increase with time up to the point where a silicate phase is precipitated.

(2) The dissolution is selective. A smaller amount of silica is released. In this case a residual hydrated glass (leached layer) should be observable by electron microscopy.

(3) The dissolution is initially selective and becomes congruent later. The dissolution of glass is selective initially and leads to the formation of a leached layer later. A further breakdown of the glassy network will maintain a constant thickness of the leached layer. Finally, the precipitation of a silica phase on the surface of the leached layer will be marked by the decreased rate of silica released to solution.

These authors experimentally altered a synthetic basaltic glass in seawater, but found no Si-rich leached layer using scanning-transmission electron microscopy (STEM) analysis. Therefore, they argued that glass alteration occurs as a uniform dissolution of the network-forming elements followed by the precipitation of authigenic material, resulting in palagonite layers.

In the present study, a combination of electron microprobe analysis (EMPA), transmission electron microscopy (TEM) and high-resolution TEM (HRTEM) and scanning electron microscopy (SEM) was used to characterize three petrographically distinct styles of altered glasses in hyaloclastites and hyalotuffs with the hope of better understanding the mechanism by which sideromelane altered and palagonite formed in these samples.

MATERIAL AND ANALYTICAL METHODS

Material and geological setting

Sample 116-4 is a well-consolidated hyalotuff from the Holocene Keanakako'i Ash of Kilauea Volcano. Palagonitization of this tuff appears to have occurred under hydrothermal conditions (<50ºC) shortly after its deposition from phreatomagmatic eruptions at the summit of Kilauea (Schiffman *et al*., 2000). A detailed description of the geological setting, petrogenesis and mineralogy was given by Schiffman *et al*. (2000, 2002).

Samples 4677 and 7231 are hyaloclastites recovered in core from the Hawaii Scientific Drilling Project's 3 km deep drill hole. The temperature at the base of this hole is <45ºC, and has probably never exceeded this in the past (Walton and Schiffman, 2003). The sample numbers refer to the depth (in feet below sea level) from which the core was recovered. The hyaloclastites are Pleistocene in age and formed from quenching of Mauna Kea surface lava flows as they entered the sea. Diagenesis, attending burial within the flanks of Mauna Kea volcano, has resulted in weak consolidation of sample 4677 and strong consolidation of sample 7231. Details on the diagenetic history, petrogenesis and mineralogy of these samples have been presented by Walton and Schiffman (2003).

Methods of analysis

For this study, the compositions of fresh glass, palagonite and smectite were investigated by EMPA. Textural analyses were performed using a variety of techniques including backscattered electron (BSE) imaging (on the electron microprobe), SEM and TEM.

EMPA and SEM. Quantitative analyses and BSE imaging were performed on a Cameca SX-100 wavelength dispersive microprobe. For quantitative analyses, the beam conditions used were 15 keV, 5 nA beam current, and a rastered spot ~5 by 5 μm. Secondary electron images were acquired on an FEI XL-30sFEG SEM equipped with an EDAX Phoenix EDS system. For SEM analyses, the samples were crushed gently, mounted on Al stubs, and carbon coated. These fractions were then studied with an FEI XL-30 FEG scanning electron microscope equipped with an EDAX Phoenix EDS X-ray microanalyzer.

https://doi.org/10.1346/CCMN.2004.0520508 Published online by Cambridge University Press

Transmission electron microscope. Transmission electron microscopy was performed using a Topcon EM 002B in the Lawrence Berkeley National Laboratory (LBNL). A thin-section was prepared for each sample. Copper rings were attached to selected areas and detached afterwards from their corresponding areas by gentle heating. The sample obtained was then thinned with a Fashione ion mill and then carbon coated for TEM observation. The microscope was operated at 200 kV. An objective aperture of 40 µm was used as a compromise between optimum amplitude and phase contrast for images. Chemical analyses were obtained using a JEM-200CX electron microscope equipped with two Kevex EDX detectors. The microscope was operated at 200 kV (TEM or STEM mode). This technique gives semiquantitative analyses with a ±10% precision with spots as small as 50 nm.

RESULTS

Petrography

Back-scattered electron (BSE) images, which show some of the essential petrographic relationships amongst fresh glass, palagonitized glass and smectite in these samples, are presented in Figure 1. Both HSDP hyaloclastites are characterized by the presence of grain coating (*e.g.* sample 4677, Figure 1a) and/or pore coating (*e.g.* sample 7231, Figure 1b) smectite. In sample 4677, besides this coating smectite, another kind of smectite-like material has been identified that seems to be replacing glass. This smectite-like material was described by Walton and Schiffman (2003) as "reddened smectite grain replacement" (or RSGR). The RSGR in this sample exhibits an alteration front into the sideromelane: the alteration intensity in glass decreases as we move from coating smectite towards sideromelane. Some tubules, apparently empty, in fresh glass (top of Figure 1a) are also present in this sample. Primary olivine grains (*i.e.* white grains in the left center of Figure 1a) are unaltered.

In sample 7231, similar features have been found. First a uniform smectite-like material layer coats the inner surface of pores (white arrow in Figure 1b). An isotropic palagonite layer (also known as gel-palagonite, Figure 1b) takes place between pore-coating smectite and glass. Zeolitic (*i.e.* phillipsite and chabazite) pore-filling cements are also found in this sample (although not seen in Figure 1b). The Kilauea sample (116-4) also contains isotropic palagonite. In this sample, the palagonite appears to form ~10–20 µm thick rinds on both the exterior and interior surfaces of ash-sized glass shards (Figure 1c). Unlike the 7231 sample, neither coating smectite nor zeolites have been found in this sample which still retains much primary porosity (*i.e.* black spaces between grains in Figure 1c).

Electron microprobe analyses

The EMPA data corresponding to sideromelane are presented in Table 1 and those corresponding to smectite-like material, RSGR and palagonite in Table 2.

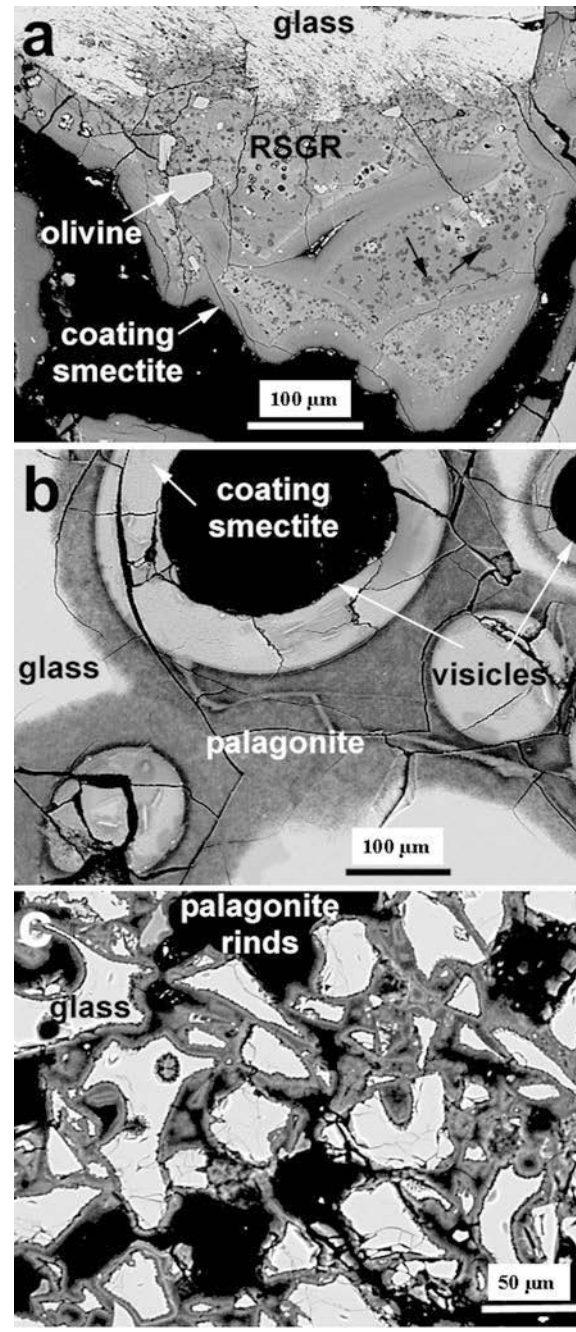

Figure 1. BSE microprobe images of (a) sample 4677 showing coating smectite, reddened smectite grain replacement (RSGR) and nodules of Ti-rich amorphous material; (b) sample 7231 showing pore-coating smectite and palagonite; and (c) sample116-4 showing palagonite rimming the glass grains.

https://doi.org/10.1346/CCMN.2004.0520508 Published online by Cambridge University Press

Table 1. EMPA microanalyses of sideromelane.

Sideromelane	Sample 4677	Sample 7231	Sample 116-4
SiO_2	49.95	51.19	49.33
TiO_2	2.73	2.30	2.42
Al_2O_3	14.29	13.90	13.40
FeO	11.36	10.50	11.13
MnO	0.15	0.15	0.06
MgO	7.83	7.02	8.33
CaO	11.04	11.06	10.34
Na_2O	2.60	2.07	2.40
K_2O	0.39	0.33	0.42
P_2O_5	0.50	0.37	0.29
Total	100.85	98.88	98.12

Sample 4677. The chemical composition of sideromelane in this sample is consistent with it being of tholeiitic affinity and olivine (not reported) is fosteritic with a Mg:Fe ratio of ~6.68. A total of 12 analyses from this sample (4677) from three different regions of the coating form of smectite are shown in Table 2: around olivine (indicated as 'C/O' in Table 2), around glass (C/G) and against the walls of the vesicles (C/V). The mean structural formula of each kind, based on 11 O, conforms to a smectite-like composition (Table 2). No systematic compositional differences have been detected between these three 'different' regions within the coating smectite. Tetrahedral and octahedral components in the coating smectite show a very constant composition with the exception of Fe which exhibits a wider range of variation than Al and Mg. The octahedral occupancy is too high for a dioctahedral smectite. Ca^{2+} is the most abundant cation in the interlayer sites of the coating smectite but Na and K are also abundant producing, along with Ca, a high interlayer charge to this smectite. The RSGR shows a very similar composition (Table 2), though its octahedral sites contain a much larger Ti content.

Sample 7231. Eleven analyses were performed on the pore-lining smectite and another eight were performed in the palagonite area. The structural formulae based on 11 O for the coating smectite in this sample indicate that Fe and Mg dominate the octahedral cations with a lesser amount of Al. As in sample 4677, the high octahedral content suggests a di-trioctahedral smectite. An unusually high interlayer charge (0.66/11O) mainly derived by Ca is also one of the characteristics of this smectite. The coating smectite in sample 7231 has a higher Ti

Table 2. Average EMPA analyses of smectite, RSGR and palagonite and their equivalent structural formulae based on 11 O.

Sample	4677				7231		116-4
Area	RSGR	C/O	C/G	C/V	palagonite	S/C	palagonite
SiO_2	45.57	49.59	50.20	49.29	43.73	45.78	45.50
TiO_2	3.08	0.03	0.03	0.03	4.13	0.16	1.06
Al_2O_3	12.49	14.08	14.30	13.58	11.62	9.21	24.57
FeO	7.22	7.88	8.18	8.61	4.51	17.41	6.68
MnO	0.15	0.16	0.14	0.18	0.04	0.28	0.08
MgO	12.53	12.85	13.12	13.50	1.24	10.23	4.26
CaO	2.45	2.48	2.56	2.20	9.98	3.56	1.27
Na_2O	0.28	0.30	0.26	0.40	0.34	0.18	0.03
K_2O	0.97	0.62	0.64	0.67	0.23	0.44	0.04
P_2O_5	0.04	0.08	0.02	0.04	0.23	0.06	0.07
Total	84.80	88.06	89.46	88.49	76.05	87.31	83.55
Structural formulae based on 11 O							
Si	3.43	3.55	3.55	3.54	3.66	3.53	3.35
^{IV}Al	0.57	0.45	0.45	0.46	0.34	0.47	0.65
^{VI}Al	0.54	0.74	0.74	0.68	0.81	0.37	1.48
Ti	0.17	0.00	0.00	0.00	0.26	0.01	0.06
Fe	0.45	0.47	0.48	0.52	0.32	1.12	0.41
Mn	0.01	0.01	0.01	0.01	0.00	0.02	0.00
Mg	1.41	1.37	1.38	1.44	0.15	1.18	0.47
Σoct.	2.58	2.60	2.61	2.66	1.54	2.70	2.42
Ca	0.20	0.19	0.19	0.17	0.89	0.29	0.10
Na	0.04	0.04	0.04	0.06	0.05	0.03	0.00
K	0.09	0.06	0.06	0.06	0.03	0.04	0.00
Int. cha.	0.53	0.48	0.48	0.45	1.87	0.66	0.21

RSGR = reddened smectite grain replacement C/O, C/G and C/V are coating smectites on olivine, glass crystals and inside the vesicles, respectively Σoct. = sum of octahedral cations.
Int. cha. = interlayer charge

https://doi.org/10.1346/CCMN.2004.0520508 Published online by Cambridge University Press

content in comparison with coating smectite in the 4677 sample. The palagonite in sample 7231 exhibits a distinctly different composition than the coating smectite, specifically higher Ca, Al and Ti contents and lower Fe and Mg contents (Table 2).

Sample 116-4. Fifteen analyses were performed on the palagonite. The average structural formula based on 11 O is listed in Table 2. The composition of the palagonite in this sample is very distinct from that in sample 7231. The Al content in the octahedral sites is higher suggesting a nearly dioctahedral smectite-like composition. However, although the Fe and Mg contents are low, the octahedral sum is still higher than is usually found in typical dioctahedral smectites. The interlayer site is dominated by Ca.

Compositional variations of smectite and palagonite

The relationship amongst the chemical components of coating smectite, RSGR and palagonite in the three samples are presented in Figure 2. The 4677 and 7231 coating smectites (indicated by open circles and diamonds, respectively, in Figure 2a,b) show no significant correlation between Fe and Mg *vs.* ^{VI}Al; Fe and Mg vary widely while ^{VI}Al remains almost constant. Palagonite from sample 116-4 reveals a good negative

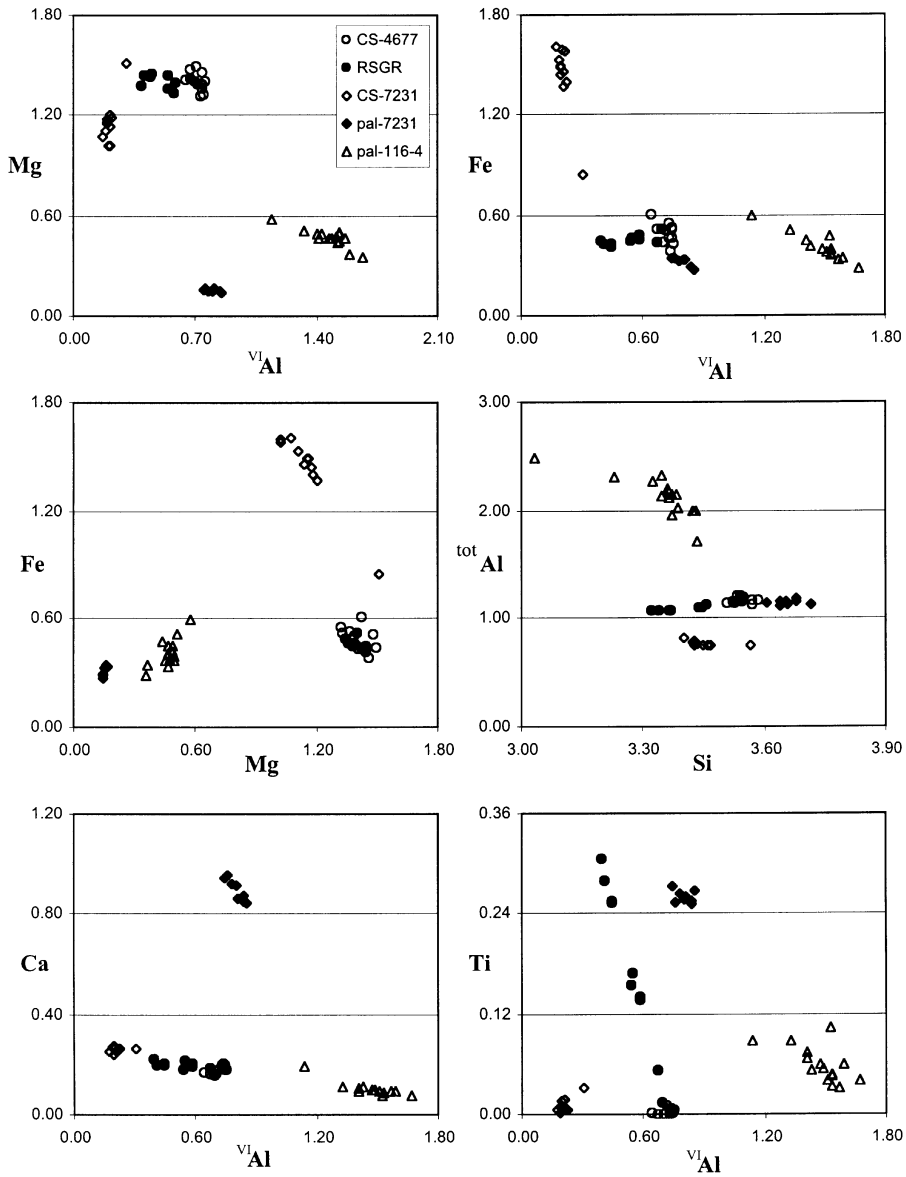

Figure 2. Chemical variation among coating smectites (CS), palagonite (pal) and reddened smectite grain replacement (RSGR). Numbers refer to the sample. ^{VI}Al and ^{tot}Al indicate octahedral and total Al content by 10 O and 2 (OH), respectively.

https://doi.org/10.1346/CCMN.2004.0520508 Published online by Cambridge University Press

correlation between these octahedral cations; both Fe and Mg decrease as ^{VI}Al increases. Conversely, Fe and Mg exhibit a negative correlation in coating smectite in sample 7231 and a positive correlation in palagonite from sample 116-4 (Figure 2c). Silicon and ^{tot}Al reveal a negative correlation in sample 116-4 but in the other samples ^{tot}Al remains constant while Si varies over a short range (Figure 2d). The Ca and Ti *vs.* ^{VI}Al show a negative correlation in palagonite from sample 116-4 and RSGR in sample 4677. However, this correlation is lacking in the coating smectites in both the 4677 and 7231 samples (Figure 2e,f). In general, the palagonite in sample 7231 shows the same characteristics as in 116-4.

A plot of the octahedral composition of coating smectite, RSGR and palagonite in the Mg-^{VI}Al-Fe ternary system shows that each sample has a distinct composition (Figure 3). Both coating smectite and RSGR from the 4677 and 7231 samples plot in the nontronite-saponite side whereas palagonites from the 116-4 and 7231 sample fall in the Al-dioctahedral smectite field where most of the analyses could be classified as Fe-rich montmorillonite (Güven, 1988). In sample 4677, the compositions of the coating smectite and the RSGR plot closely. The compositional evolution from glass to coating smectite, in the two samples 4677 and 7231, has an opposite direction (*i.e.* towards Mg enrichment in sample 4677 and Fe enrichment in sample 7231). However, in the palagonites from both the 116-4 and 7231 samples, the evolution entails Al enrichment and Fe and Mg depletion.

Scanning electron microscopy

The SEM images of these three samples are presented in Figure 4. All the components described in this section were identified on the basis of EDX microanalysis and similarities with BSE images. Figure 4a shows coating smectite, exhibiting a flake-like morphology on the surface of glass and phenocrysts of olivine in sample 4677. The RSGR in this sample (Figure 4b) exhibits a distinctly different morphology, with the smectite intimately intergrown with the Ti-rich nodular inclusions producing a sponge-like texture.

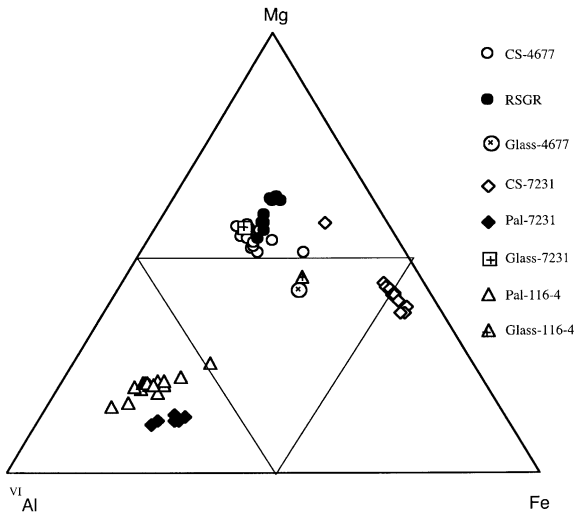

Figure 3. Plot in the Mg-^{VI}Al-Fe ternary diagram of the octahedral composition of coating smectites, palagonites, reddened smectite grain replacement (same symbols as in Figure 2) and glass. The numbers refer to the samples. Glass compositions were plotted after readjusting to 11 O.

Figure 4c shows the texture of vesicle linings (or coatings) in the 7231 sample. Material on the vesicle walls (Figure 4c) is identified as smectite whereas zeolite fills the remaining interior pore space (both smectite and zeolite are identified on the basis of EDX analysis). A thin layer of palagonite occupies the region between the smectite pore linings and the fresh glass (Figure 4c). The palagonite has a packet-like structure with individual 'layers' a few nm thick (Figure 4d). Similar textures are observed in sample 116-4. This sample has empty vesicles with a 5 μm thick palagonite rind, with a flake-like texture, lining the walls of the vesicles (Figure 4e). Unlike the coating in other samples, the boundary between glass and the palagonitic linings is not sharp. As can be seen in more detail in Figure 4f, the alteration of sideromelane seems to have a front that grows inward from the surface of the glass; in fact, the size of pores and smectite-like particles decreases moving inward to the glass. As in sample 7231, the palgonite exhibits a packet-like morphology (a few nm thick).

Transmission electron microscopy

Low-magnification TEM images (Figure 5a) show that the coating smectite in sample 4677 is formed exclusively by fibrous, clay-like material. These particles vary in thickness up to 50 nm. No other clays, amorphous material or structures were found in between these coating smectites. Lattice-fringe images (Figure 5b) show that these particles are formed by several, slightly curved, 1 nm layers. The TEM images obtained from the RSGR domains are similar to those from the coating smectite. However, the fibrous particles look to be thinner than those in the coating smectite (Figure 5c). Moreover, some rounded nodules corresponding to Ti-rich amorphous materials were found in isolated domains between smectite fibers (Figure 6). The energy-dispersive X-ray (EDX) analysis (not shown) indicates that the Ti-rich material consists mainly of Ti, Si and Ca, with lesser amounts of Al, Mg and Fe, consistent with the wavelength-dispersive microprobe analyses of coarser nodules presented in Table 3 of Walton and Schiffman (2003).

The TEM images of sample 7231 are very similar to those of sample 4677. There is a clear boundary separating coating smectite from palagonite (Figure 7a). Both the coating smectite and palagonite show clay-like fibrous structure. However, as can be clearly seen in Figure 7a, the two zones are different; the

https://doi.org/10.1346/CCMN.2004.0520508 Published online by Cambridge University Press

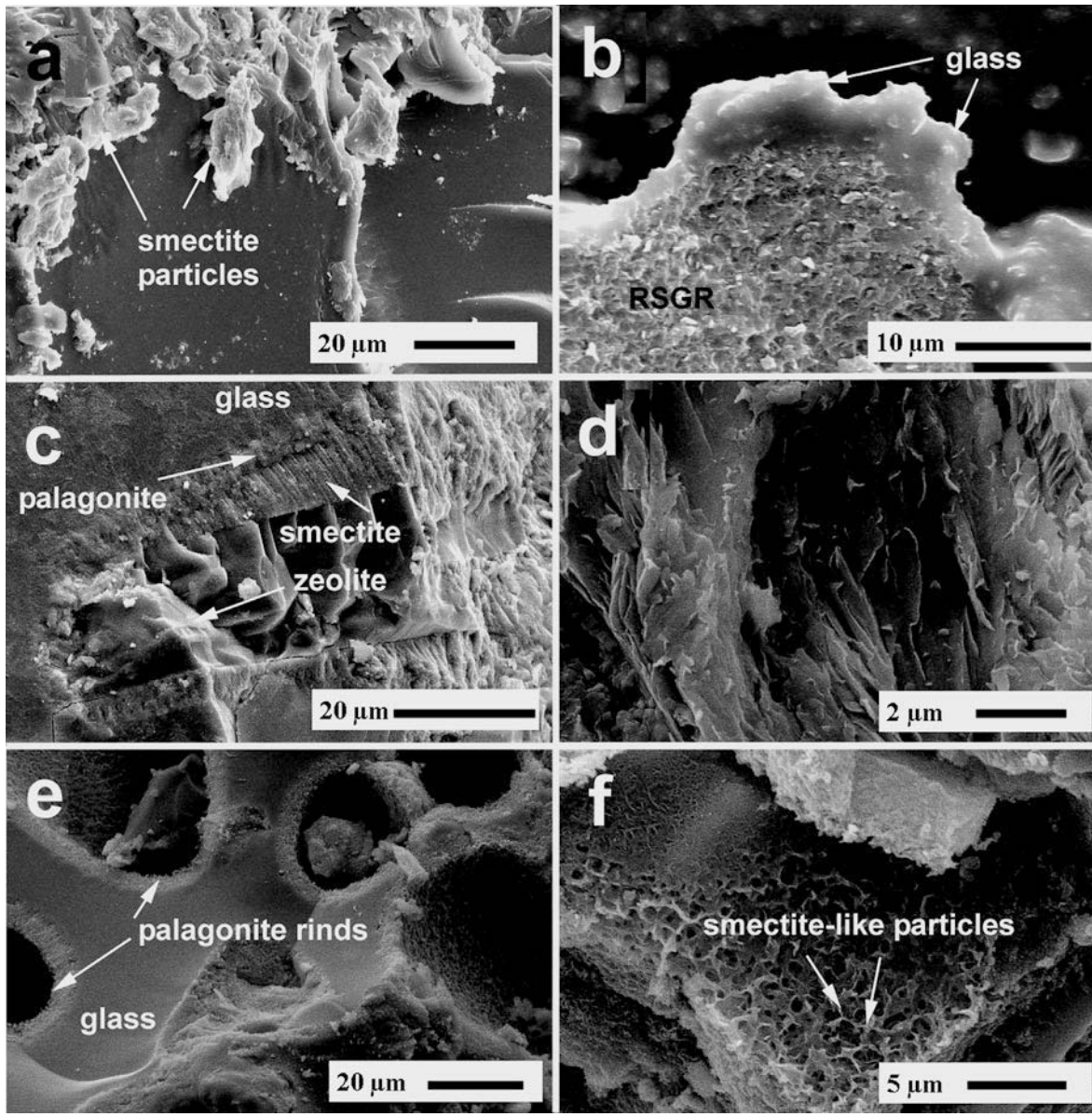

Figure 4. SEM images of (a) smectite from sample 4677 coating the surface of olivine, (b) sample 4677 showing the boundary limit between RSGR and glass, (c) sample 7231 showing the typical filling sequence in the vesicles, (d) detail of the palagonite area in (c), (e) sample 116-4 showing palagonite rinds, and (f) detail of the palagonite rinds.

fibers are thicker in the coating smectite than in palagonite. The electron diffraction patterns obtained from the palagonite area (Figure 7b) indicate that it is amorphous to very poorly crystalline (very diffused ring). Lattice-fringe images offer more detail about the thickness and crystallinity of these two separated domains; the coating smectite area is formed by individual packets of ~15 layers each. The same structure can also be seen in the palagonite (Figure 7d). However, the lattice-fringe image shows poorly defined 1 nm layers generally individualized into packets of only 1 or 2 nm. However, in some areas, the stacking appears to be up to as much as 9 layers thick (Figure 7d).

The TEM image of sample 116-4 (Figure 8) shows the same basic fibrous structure as seen in the other samples. However, some differences should be emphasized. The fibrous clay-like material (20–50 nm, in general) is completely amorphous (SAED not shown). Unlike the other samples, the clay-like material in this sample shows a dissolution front (indicated by the dashed line in Figure 9) as mentioned before for SEM images. Also, there is no sharp boundary between palagonite and glass, but rather a progressive etching

https://doi.org/10.1346/CCMN.2004.0520508 Published online by Cambridge University Press

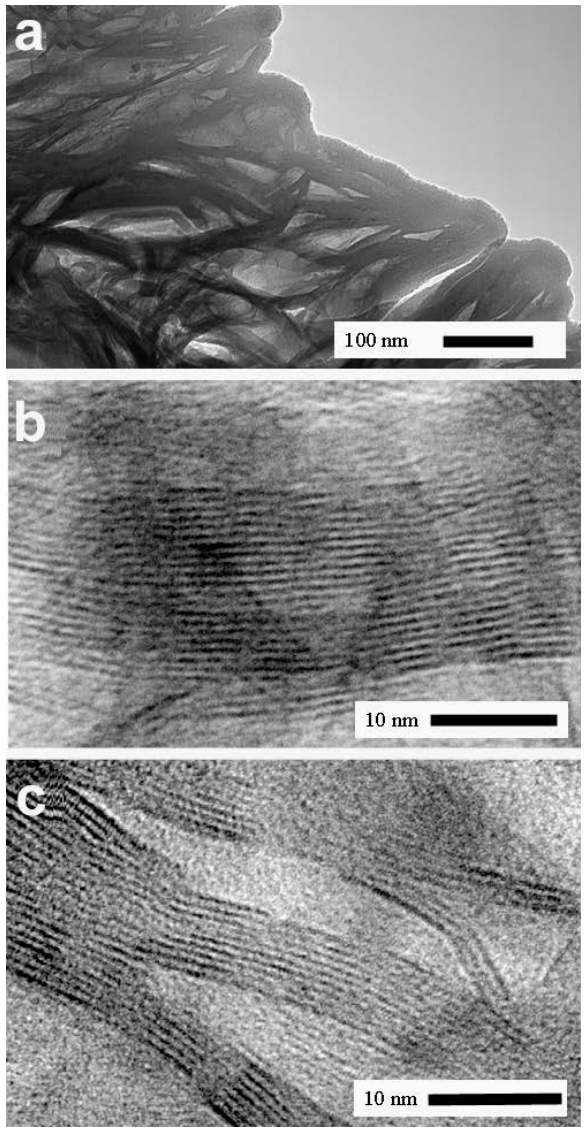

Figure 5. TEM images of sample 4677 showing (a) coating smectite, and HRTEM images of (b) coating smectite and (c) RSGR.

inwards to the glass (Figure 9) marked by the individualization of leached layers in the fracture zones of the fresh glass that grow in thickness approaching the interface with palagonite.

DISCUSSION

Clay minerals (mainly smectite and amorphous materials) are present in three different microenvironments in the samples studied: (1) as mainly crystalline coatings on the surface of glass crystals, or the walls of vesicles; (2) as RSGR replacing glass; or (3) as a poorly crystalline material in palagonite which has replaced glass. Differences in the compositional variations of smectite between samples and microenvironments indicate that smectite formation during the very low-temperature alteration of basaltic glass is different from one sample to another and from one microenvironment to another in a given sample (*e.g.* between coating smectite and smectite-like material in palagonite). Thus, different factors appear to affect the process of palagonitization.

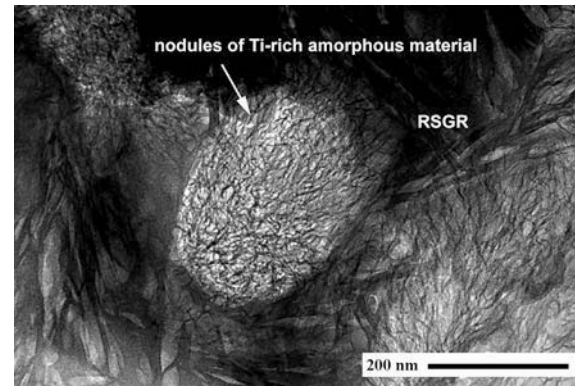

Figure 6. Low-magnification TEM image of fine-grained smectite and Ti-rich amorphous material (arrow) forming the matrix in the RSGR area from sample 4677.

Smectite and palagonite classification in the Mg-^{VI}Al-Fe ternary system

The EMPa analyses show that coating smectite and RSGR, in samples 4677 and 7231, have a composition intermediate between saponite and nontronite (Figure 3). Although the octahedral sum suggests di-trioctahedral smectites, no similar compositions have ever been reported in the literature. Crovisier *et al*. (1992) indicated that it is very likely that two chemically different clay minerals (saponite and nontronite) can form at equilibrium with each other during alteration of basaltic glass by meteoritic waters. Although the coexistence of two different smectite phases may be possible, the means by which this might happen is still unclear. The microscale association of dioctahedral nontronite and trioctahedral saponite has also been reported by Crovisier *et al*. (1987) and Zhou and Fyfe (1992). The presence of smectite interstratified with Fe-Mg rich clays has been reported (*i.e*. Drief *et al*., 2001). However, the only clay phase identified has a 1 nm spacing. Therefore, the compositions could be explained as a mechanical intergrowth and/or an interstratification of two different smectites: one dioctahedral (*i.e*. nontronite) and one trioctahedral (*i.e*. saponite or stevensite) or simply as a true di-trioctahedral smectite.

The chemical composition of palagonite, in the 116-4 sample, corresponds to an Fe-rich montmorillonite (Figure 3). On the other hand, palagonite from sample 7231 shows a completely different composition from the coating smectite from the same sample. This palagonite is more aluminous but still very different from a smectite-like composition. Nevertheless, the plots of octahedral cations in the Mg-^{VI}Al-Fe ternary system fall

https://doi.org/10.1346/CCMN.2004.0520508 Published online by Cambridge University Press

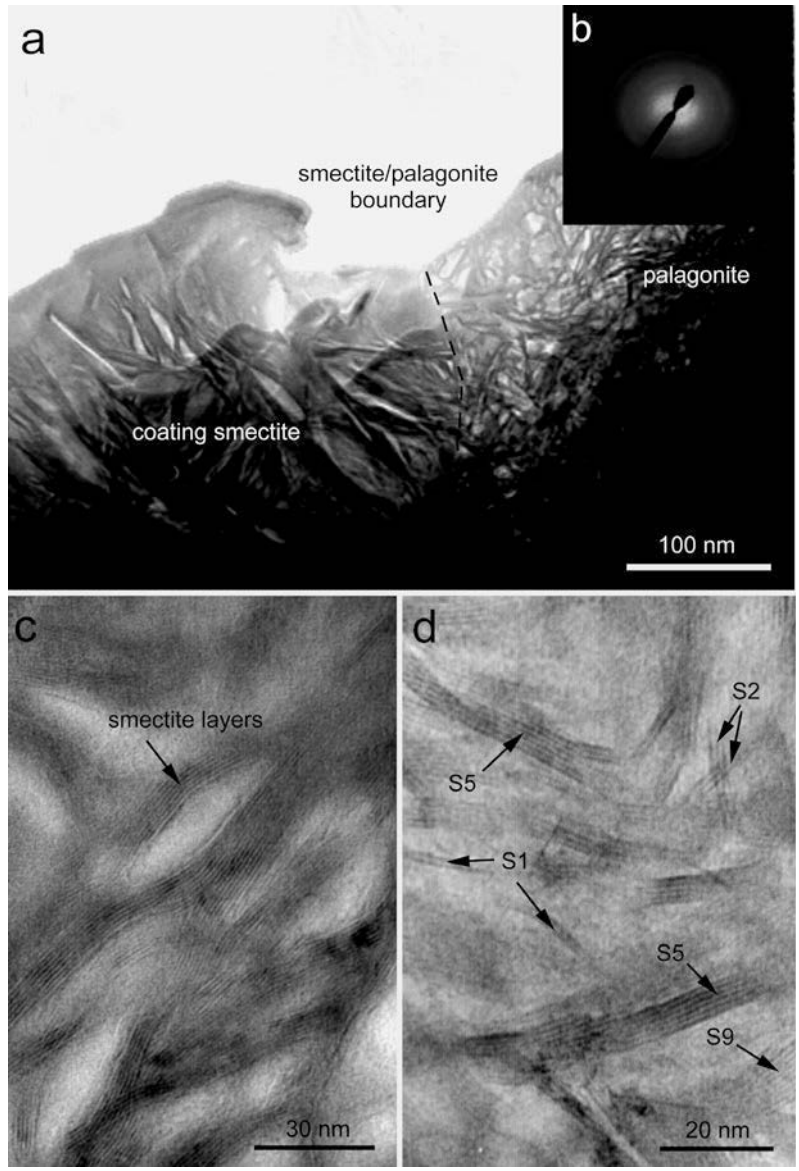

Figure 7. TEM images of sample 7231 showing: (a) the boundary limit (dotted line) between coating smectite and palagonite; (b) electron diffraction taken in the palagonite area; (c) HRTEM showing a lattice-fringe image of well crystallized smectite corresponding to the coating smectite area; and (d) lattice-fringe image of smectite-like material found in the palagonite area showing different layer stacking (*i.e.* S2 = two layers of 1 nm each).

in the field of Al-dioctahedral smectites (Figure 3), close to the palagonite from sample 116-4.

Amorphous material

The presence of the Ti-rich X-ray amorphous material is presumably due to the semi-closed system in which smectite precipitates as RSGR. Some elements (*e.g.* Ti, Ca) that do not contribute to smectite nucleation are not removed by solution. The Ti is the least soluble element during palagonitization and accumulates along with other elements (*e.g.* Ca) to form this amorphous material, creating fine-grained domains which are a mixture of smectite and X-ray amorphous material. This is why the EMPA of the RSGR domains invariably indicates a Ti-rich smectite. Moreover, the Ti *vs.* ^{VI}Al in this material exhibits a very clear negative correlation (Figure 2f) reflecting a mechanical mixture between smectite and the Ti-rich amorphous material.

Mechanism of palagonite and smectite formation

Palagonite. The palagonitization mechanism is still not well understood in spite of numerous experimental studies of synthetic glass dissolution (Hench, 1975; Scholze, 1982; Conradt and Scholze, 1984). Although it

https://doi.org/10.1346/CCMN.2004.0520508 Published online by Cambridge University Press

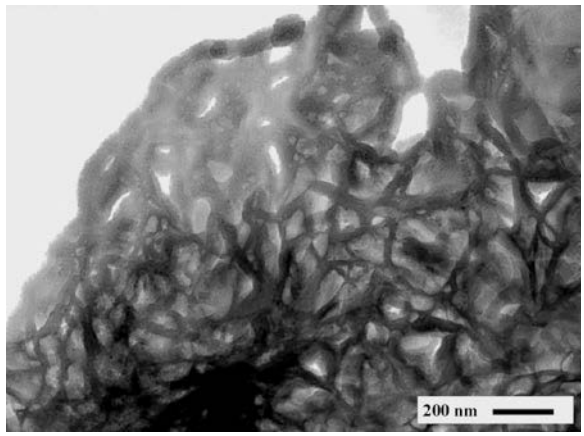

Figure 8. TEM image showing the typical texture of palagonite from sample 116-4 with interconnected, anastomosing smectite-like material.

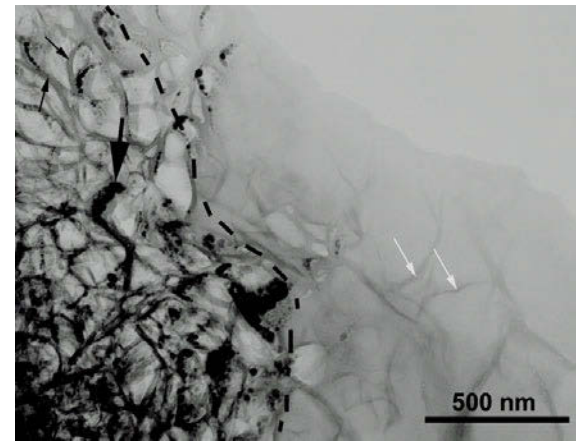

Figure 9. TEM image of sample 116-4 showing the dissolution front (dashed line) growing inwards in the glass. Thin black and white arrows indicate previously and newly formed leached layers, respectively, the thicker arrow indicates water bubbles formed by interaction with the electron beam.

is generally accepted today that a dissolution-precipitation mechanism is responsible for the alteration of sideromelane to palagonite (Berger *et al*., 1987; Crovisier *et al*., 1987; Daux *et al*., 1994; Jercinovic *et al*., 1990; Zhou and Fyfe, 1989) the main question remains whether the dissolution is congruent or selective (non-stoichiometric). Congruent dissolution can be readily characterized in experimental studies by monitoring elemental release from glass into aqueous solution (*e.g*. linear release of silica with time at constant pH, Crovisier *et al*., 1987). However, non-stoichiometric dissolution is more difficult to characterize because solution chemistry can be controlled by other reactions that occur on the surface of glass such as: (1) formation of a superficial leached layer on the glass after diffusion of alkaline and alkaline earth elements; or (2) precipitation of a surface layer after a total breakdown of the glass. According to Crovisier (1987), both the silica-rich product (that could contain other elements like Mg and Fe) and the superficial leached layer must be observable by electron microscopy.

In order to understand better the mechanism of palagonite formation, it is important to distinguish between the major steps that take place during the alteration of sideromelane. In Figure 10 we summarized the successive events that take place during the palagonitization process. It appears (from Figure 9) that the first step in the process entails the formation of a fracture complex that allows water access to the glass (Figure 10a). A selective (non-stoichiometric) dissolution takes place in the fracture zone in the contact area between glass and water. The hydration and replacement of glass during the palgonitization process is apparently accompanied by the formation of a 1–4 nm thick leached layer (Figure 10b). Unlike the results found by Crovisier *et al*. (1987) the material found to fill these fractures is completely amorphous as indicated by SAED and HRTEM. This leached layer maintains its spatial relationship with the fractures even in more advanced stages of alteration (Figure 10c) where the microfratures have become interconnected. The resultant 'vein-like' texture can be attributed to leached layers formed in pre-existing microfractures. In more evolved stages the palagonite will be formed exclusively from these Si-Al-enriched leached layers which have probably already transformed, at least partly, into smectite. These same textural and chemical characteristics are also found in the palagonite from sample 7231. A similar growth mechanism for smectite from leached layers under experimental hydrothermal conditions has been reported previously (*e.g*. Kawano and Tomita, 1994). Therefore, we assume that palagonite forms through an incongruent dissolution that leads to the formation of leached layers that subsequently convert to smectite.

Temperature, pH and chemistry solution are among the most important factors controlling congruent *vs*. selective dissolution. Therefore, it is difficult to compare congruent *vs*. incongruent dissolution mechanisms of basaltic glass on the basis of the experiments reported in the literature. Many experiments dealing with the mechanism of palagonitization were carried out under different experimental conditions. Berger *et al*. (1987) experiments took place at high temperature (*i.e*. 350ºC) with 'modified' seawater, Crovisier *et al*. (1987) at low temperatures (*i.e*. 0 to 60ºC) with artificial seawater solution, and Gislason and Eugster (1987) at low temperatures (*i.e*. 45–65ºC) with meteoric water. Also, the pH and solution/solid ratio were different in these experiments. Thus, the results discussed in this paper may not be the same in other samples which have experienced different alteration conditions.

Coating smectite. The SEM and backscattered images show that the boundaries between coating smectite and RSGR, olivine and palagonite are very sharp

https://doi.org/10.1346/CCMN.2004.0520508 Published online by Cambridge University Press

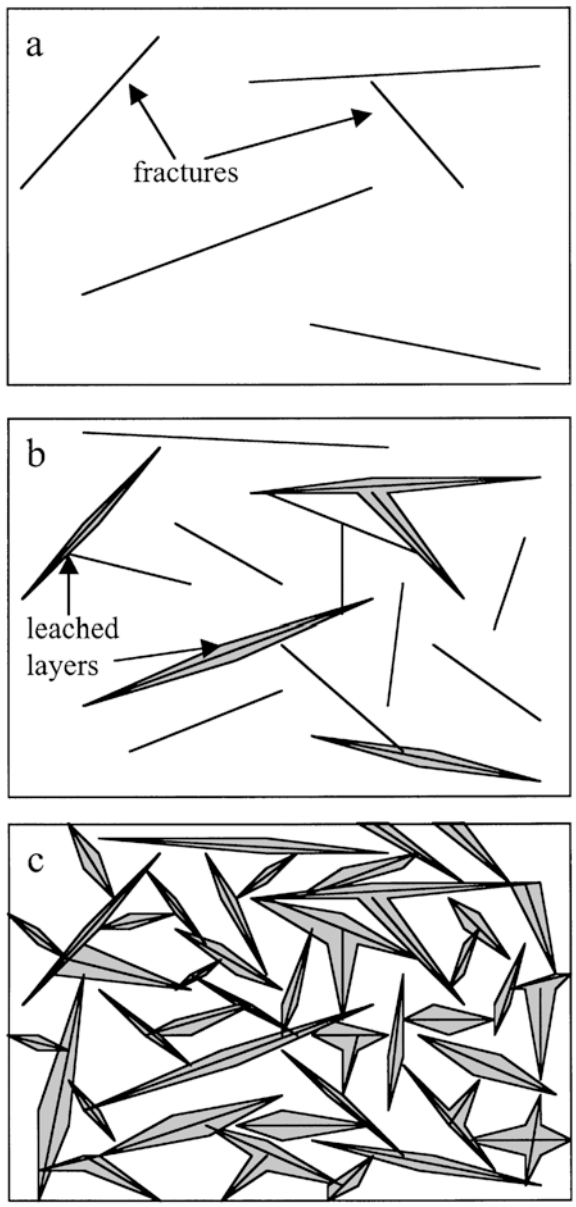

Figure 10. Schematic model of the palagonitization process by: (a) formation of a fracture complex zone followed by (b) selective dissolution of glass which leads to the formation of leached layers which (c) grow in size and transform into a smectite-like material.

(Figures 1a,b and 4a,c). Moreover, the coating smectite displays a uniform appearance and thickness unlike palagonite in samples 116-4 and 7231 and RSGR in sample 4677 which display a progressive front of alteration inwards to the glass. The HRTEM data show that coating smectites consist exclusively of crystalline smectite-like material. On the other hand, coating smectites from three different microenvironments in sample 4677 (Table 2) have essentially the same composition. This suggests that smectite composition does not depend on the 'hosting material' (*e.g.* olivine or glass) but rather on the chemistry of the solution from which this mineral precipitates. In the same way, the chemical composition of sideromelane as compared to that of coating smectite, from sample 4677, indicates that the main compositional changes accompanying smectite formation from glass is the loss of Ca, Ti and Na and the gain of Mg. The gain of Mg can be accomplished either by dissolution of olivine or seawater.

RSGR. One of the most intriguing findings of this study is that within the same sample (4677) the coating smectite and RSGR have such similar compositions despite the differences in microenvironments in which they have formed. With the exception of Ti, the chemical compositions of these two forms of smectite are nearly identical. The high Mg content in the RSGR indicates that at least a limited amount of solution transportation through the coating smectite layer has occurred to supply smectite with Mg during its precipitation.

In addition, the RSGR does not display a uniform thickness of glass replacement similar to the manner that the coating smectite rims glass (Figure 1a). This implies that the RSGR forms through a progressive dissolution of glass followed by the precipitation of smectite along with the observed Ti-rich amorphous materials. These observations indicate that the RSGR formation occurs under nearly identical conditions to the coating smectite.

CONCLUSIONS

(1) Very low-temperature alteration of glass in hyaloclastites and hyalotuffs proceeds by (a) dissolution of glass and olivine crystals, resulting in precipitation of crystalline smectite as grain and pore coatings; (b) replacement of glass by smectite which results in a mechanical mixture of crystalline smectite and amorphous materials; and (c) selective dissolution of glass resulting in the formation of leached layers that form the palagonite – an amorphous to poorly crystalline smectite-like material.

(2) Coating smectite and RSGR show an intermediate composition between the two end-members saponite and notronite. This composition could correspond to a mechanical intergrowth and/or an interstratification of two different smectites: one dioctahedral (*i.e.* nontronite) and one trioctahedral (*i.e.* saponite or stevensite) or simply to a true di-trioctahedral smectite. However, palagonite from hyalotuffs reveals an Fe-rich montmorillonite-like composition.

(3) Smectites from hyaloclastites corresponding to pore and grain coatings seem to have formed under the same conditions. The most important process in their formation from glass is the loss of Ca, Ti and Na and gain of Mg. The Mg can be supplied by olivine, glass or seawater in both the 4677 and 7231 samples. These smectites precipitate in the form of flakes on the surface

https://doi.org/10.1346/CCMN.2004.0520508 Published online by Cambridge University Press

of glass shards or as fine-grained smectite along with Ti-rich X-ray amorphous material (RSGR). However, the most important process in the palagonite formation in hyalotuffs is the loss of Fe, Mg and Ca with a concomitant gain of Al. Such a process seems to be favored by the formation of a leached layer in the fracture zone into the glass.

ACKNOWLEDGMENTS

Primary support for this research was provided by the NSF grant EAR 0125666, NASA grant MFRP-NRA 02-OSS-01, and the "Plan Propio" grant of the University of Granada. The authors thank R.A. Eggleton, J. Honnorez and Associate Editor, Warren Huff, for constructive criticism of the initial version of the manuscript. We acknowledge Norm Winter (UCD Geology) for preparation of polished thin-sections. The TEM work at the National Center for Electron Microscopy at the LBNL was supported by the Office of Basic Energy Sciences of the US Department of Energy under Contract No. DE-AC03-76SF00098. We thank Tony Walton (Kansas University) for discussions on the alteration of the HSDP palagonites.

REFERENCES

Bell, J.F., McSween, H.Y., Jr, Crisp, J.A. Morris, R.V. and Murchie, S.L. (2000) Mineralogic and compositional properties of Martian soil and dust: Results from Pathfinder. *Journal of Geophysical Research*, **105**, 1721–1755.

Berger, G., Schott, J. and Loubet, M. (1987) Fundamental processes controlling the first stage alteration of a basalt glass by seawater: an experimental study between 200º and 320ºC. *Earth and Planetary Science Letters*, **84**, 431–445.

Conradt, R. and Scholze, H. (1984) Glass corrosion in aqueous media – a still unsolved problem? *Revista della Stazione Sperimentale del Vetro, Murano (Italy)*, **5**, 73–77.

Crovisier, J.L., Honnorez, J. and Eberhart, J.P. (1987) Dissolution of basaltic glass in sea water; mechanism and rate. *Geochimica et Cosmochimica Acta*, **51**, 2977–2990.

Crovisier, J.L., Honnorez, J., Fritz, B. and Petit, J.C. (1992) Dissolution of subglacial volcanic glasses from Iceland: laboratory study and modeling. *Applied Geochemistry, Supplement*, **1**, 55–81.

Daux, V., Crovisier, J.L., Hemond, C. and Petit, J.C. (1994) Geochemical evolution of basaltic rocks subjected to weathering: fate of the major elements, rare earth elements, and thorium. *Geochimica et Cosmochimica Acta*, **58**, 4941–4954.

Drief, A., Nieto, F. and Sanchez-Navas, A. (2001) Experimental clay-mineral formation from a subvolcanic rock by interaction with 1 M NaOH solution at room temperature. *Clays and Clay Minerals*, **49**, 92–106.

Eggleton, R.A. and Keller, J. (1982) The palagonitization of limburgite glass – a TEM study. *Neues Jahrbuch für Mineralogie Montashefte*, 321–336.

Fisher, R.V. and Schmincke, H.-U. (1984) Alteration of volcanic glass. Pp. 312–345 in: *Pyroclastic Rocks*. Springer, Berlin, Heidelberg, New York.

Furnes, H. (1984) Chemical-changes during progressive subaerial palagonitization of a subglacial olivine tholeiite hyaloclastite – a microprobe study. *Chemical Geology*, **43**, 271–285.

Gislason, S.R. and Eugster, H.P. (1987) Meteoric water-basalt interaction I: a laboratory study. *Geochimica et Cosmochimica Acta*, **51**, 2827–2840.

Gooding, J.L. and Keil, K. (1978) Alteration of glass as a possible source of clays on Mars. *Geophysics Research Letters*, **5**, 727–730.

Güven, N. (1988) Smectite. Pp. 497–559 in: *Hydrous Phyllosilicates* (S.W. Bailey, editor). Reviews in Mineralogy, **19**. Mineralogical Society of America, Washington, D.C.

Hay, R.L. and Iijima, A. (1968a) Nature and origin of palagonitic tuffs of the Honolulu Group on oahu, Hawaii. *Geological Society of America Memoir*, **116**, 338–376.

Hay, R.L. and Iijima, A. (1968b) Petrology of palagonite tuffs of Koko craters, Oahu, Hawaii. *Contributions to Mineralgy and Petrology*, **17**, 141–154.

Hench, L.L. (1975) Characterization of glass corrosion and durability. *Journal of Non-Crystalline Solids*, **19**, 27–39.

Honnorez, J. (1978) Generation of phillipsites by palagonitization of basaltic glass in sea water and the origin of K-rich deep-sea deposits. Pp. 245–258 in: *Natural Zeolites: Occurrence, Properties, Use* (L.B. Sand and F.A. Mumpton, editors). Pergamon, New York.

Honnorez, J. (1981) The aging of the oceanic lithosphere. Pp. 525–587 in: *The Oceanic Lithosphere* (C. Emiliani, editor). John Wiley, New York.

Jakobsson, S.P. (1972) On the consolidation and palagonitization of the tephra of the Surtsey volcanic island, Iceland. *Surtsey Research Progress Report*, **6**, 1–8.

Jercinovic, M.J., Keil, K., Smith, M.R. and Schmitt, R.A. (1990) Alteration of basaltic glasses from north-central British Colombia, Canada. *Geochimica et Cosmochimica Acta*, **54**, 2679–2696.

Kawano, M. and Tomita, K. (1994) Growth of smectite from leached layer during experimental alteration of albite. *Clays and Clay Minerals*, **42**, 7–17.

Moore, J.G. (1966) Rate of palagonitization of submarine basalt adjacent to Hawaii. *US Geological Survey Professional Paper*, **550-D**, pp. D163–D171.

Morris, R.V., Golden, D.C., Ming, D.W., Shelfer, T.D., Jorgensen, L.C., Bell, J.F., Graff, T.G. and Mertzmen, S.A. (2001) Phyllosilicate-poor palagonite dust from Mauna Kea Volcano (Hawaii): A mineralogical analogue for magnetic Martian dust? *Journal of Geophysical Research*, **105 E1**, 1757–1817.

Peacock, M.A. (1926) The petrology of Iceland, part 1. The basic tuffs. *Transactions of the Royal Society of Edinburgh*, **55**, 53–76.

Schiffman, P., Spero, H.J., Southard, R.J. and Swanson, D.A. (2000) Controls on palaonitization versus pedogenic weathering of basaltic tephra: evidence from the consolidation and geochemistry of the Keanakako'I Ash Member, Kilauea Volcano, *Geochemistry Geophysics Geosystems*, **1**, Paper number 2000GC000068.

Schiffman, P., Southard, R.J., Eberl, D.D. and Bishop J.L. (2002) Distinguishing palagonitized from pedogenically-altered basaltic Hawaiian tephra: mineralogic and geochemical criteria. *Volcano/Ice Interactions on Earth and Mars.* Special issue of *Journal of the Geological Society*, **202**, 393–405.

Scholze, H. (1982) Chemical durability of glasses. *Journal of Non-Crystalline Solids*, **52**, 91–103.

Singer, A. (1974) Mineralogy of palagonitic material from the Golan Heights, Israel. *Clays and Clay Minerals* **22**, 231–240.

Singer, A. and Banin, A. (1990) Characteristics and mode of formation of palagonite: a review. *Proceedings of the 9th International Clay Conference, Strasbourg*, pp. 173–181.

Stokes, K.R. (1971) Further investigations into the nature of the materials chlorophaeite and palagonite. *Mineralogical Magazine*, **38**, 205–214.

Stroncik, N.A. and Schmincke, H.-U. (2001) Evolution of palagonite: crystallisation, chemical changes and element

budget. *Geochemistry Geophysics Geosystems*, **2**, Paper number 2000GC000102.

Thomassin, J.H., Baillif, P. and Touray, J.C. (1983) Comparaison des mechanismes d'alteration des verres basaltiques et andésitiques dans l'eau de mer a 90ºC, 1 bar (entre 15 minutes et 9 mois). *Bulletin de la Société Géologique de France*, **36**, 2–3, 173–186.

Thorseth, I.H., Furnes, H. and Tumyr, O. (1991) A textural and chemical study of Icelandic palagonite of varied composition and its bearing on the mechanism of the glass-palagonite transformation. *Geochimica et Cosmochimica Acta*, **55**, 731–749.

Von Waltershausen, W.S. (1845) Über die submarine Ausbrüche in der tertiären Formation des Val di Noto im Vergleich mit verwandten Erscheinungen am Ätna. *Göttinger Studien*, **1**, 371–431.

Walton, A.W. and Schiffman, P. (2003) Alteration of hyaloclastites in the HSDP 2 Phase 1 Drill Core: (I) Description and Paragenesis. *Geochemistry Geophysics Geosystems*, **4**, Paper number 2002GC000368.

Zhou, Z. and Fyfe, W.S. (1989) Palagonitization of basaltic glass from DSDP site-335, LEG-37 – textures, chemical composition, and mechanism of formation. *American Mineralogist*, **74**, 1045–1053.

Zhou, Z.H., Fyfe, W.S., Tazaki, K. and Vandergaast, S.J. (1992) The structural characteristics of palagonite from DSDP Site-335. *The Canadian Mineralogist*, **30**, 75–81.

(*Received 1 December 2003; revised 21 April 2004; Ms. 863; A.E. Warren D. Huff*)